Oscillation of the Ionosphere Caused by the 2022 Tonga Volcanic Eruption Observed with SuperDARN Radars

Jiaojiao Zhang[1,2], Jiyao Xu[1,2], Wei Wang[1,2], Guojun Wang[1,2], J. Michael Ruohoniemi[3], Atsuki Shinbori[4], Nozomu Nishitani[4], Chi Wang[1,2], Xiang Deng[1], Ailan Lan[1,2], and Jingye Yan[1,2]

[1]State Key Laboratory of Space Weather, National Space Science Center, Chinese Academy of Sciences, Beijing, China
[2]University of Chinese Academy of Sciences, Beijing, China
[3]Center for Space Science and Engineering Research (Space@VT), Virginia Polytechnic Institute and State University, Blacksburg, VA, USA
[4]Institute for Space-Earth Environmental Research, Nagoya University, Nagoya, Japan

Key Points:

- Enhanced ionospheric irregularities with highly variable velocities were observed after the Tonga volcanic eruption.
- The maximum amplitude of the line-of-sight velocity of the ionospheric oscillation approached 150 m/s in E layer.
- The ionosphere was displaced upwards by as much as 100 km.

Corresponding author: Jiaojiao Zhang, `jjzhang@spaceweather.ac.cn`

Abstract

On 15 January 2022, the submarine volcano on the southwest Pacific island of Tonga violently erupted. Thus far, the ionospheric oscillation features caused by the volcanic eruption have not been identified. Here, the field-aligned electron density irregularities in the ionosphere detected by Super Dual Auroral Radar Network (SuperDARN) radars are employed as tracers to analyse ionospheric oscillation in the Northern Hemisphere caused by the volcanic eruption in Tonga. Due to the magnetic field conjugate effect, the ionospheric oscillations were observed much earlier than expected, and the maximum negative line-of-sight (LOS) velocity of the ionospheric oscillation exceeded 100 m/s in the F layer. After the surface air pressure wave arrived, the maximum LOS velocity in the E layer approached 150 m/s. The ionosphere also experienced a maximum upwards displacement of 100 km. This work provides a new perspective for understanding the strong ionospheric oscillation caused by geological hazards observed on Earth.

Plain Language Summary

On 15 January 2022, an underwater volcano on the southwest Pacific island of Tonga erupted, triggering significant disturbances on the surface and in the ionosphere that propagated worldwide. The oscillation features of the ionosphere caused by the volcanic eruption have not been identified. The volcanic eruption caused numerous irregularities in the ionosphere. These irregularities move with the ionosphere similar to how leaves move in a rough sea. In this study, the ionospheric irregularities were observed and employed as tracers to analyse the ionospheric oscillation. It was observed that the ionospheric oscillation exhibited different features before and after the arrival of the surface air pressure wave, including the maximum line-of-sight (LOS) velocity, the altitude of the maximum LOS velocity, and the propagation direction. The amplitudes of the LOS velocities of the ionospheric fluctuations approached 150 m/s, and the ionosphere experienced a maximum upwards displacement of 100 km, which is the strongest ionospheric fluctuation caused by geological hazards ever observed.

1 Introduction

At 04:14:45 UTC on 15 January, 2022, the Hunga Tonga-Hunga Ha'apai submarine volcano (hereafter referred to as the Tonga volcano, which is centred at 20.546°S, 175.390°W, explosively erupted. Immense ripples on the sea surface and in the atmosphere rapidly spread outward. The volcanic explosivity index (VEL) was estimated to be 6, indicating that this eruption was one of the largest volcanic eruptions recorded in the modern era (Poli & Shapiro, 2022). The volcanic eruption released a large amount of material and energy into the atmosphere, with the highest overshooting tops of the volcanic plume reaching the lower mesosphere at an altitude of $\sim$ 55 km according to satellite imagery (Carr et al., 2022). The waves triggered by the Tonga volcanic eruption on the surface and in the ionosphere were observed worldwide by various ground- and space-based instrumentation (Adam, 2022; Wright et al., 2022; X. Liu et al., 2022).

It is well known that volcanic eruptions and earthquakes can produce measurable ionospheric waves that travel thousands of kilometres (Roberts et al., 1982). Previous studies on ionospheric disturbances caused by volcanic eruptions, earthquakes, or tsunamis mainly involved TEC variations and horizontal phase velocities of the waves (C. H. Liu et al., 1982; Heki, 2006; Dautermann et al., 2009), there are rare direct observations about the ionospheric oscillation velocity or amplitude caused by these natural hazards. After the Tonga vocanic eruption, the dense Global Navigation Satellite System (GNSS) receiver network was selected to rapidly analyse the total electron content (TEC) perturbations associated with the volcanic eruption. Themens et al. (2022) identified two large-scale traveling ionospheric disturbances (LSTIDs) with initial speeds of 950

m/s and 555 m/s. Zhang et al. (2022) discovered that the radial two-way disturbance propagation along the entire great circle lasted 4 days. This observation shows that the waves travelled around the globe three times as Lamb waves with primary speeds in the range of 300-350 m/s. Lin et al. (2022) observed the simultaneous occurrence of TIDs in Australia and Japan between 0800 and 1000 universal time (UT) on 15 January 2022. TIDs observed in Japan are attributed to the magnetic field conjugate effect. However, the effects on the ionospheric oscillations have not been demonstrated.

Field-aligned electron density irregularities are small-scale density structures in the ionospheric plasma. When the ionosphere fluctuates, these structures move with the ionosphere. Thus, the ionospheric irregularities are good tracers for ionospheric movement. Super Dual Auroral Radar Network (SuperDARN) radars are powerful tools for observing the motion of irregularities in the ionosphere (Chisham et al., 2007; Nishitani et al., 2019). These radars receive backscatter echoes from irregularities in the D, E and F layers of the ionosphere. Nishitani et al. (2011) observed the Doppler velocities of ground/sea scatter echoes with a magnitude of 100 m/s that lasted for several minutes after the 2011 Tohoku Earthquake by using high temporal resolution (8s) data from (SuperDARN) Hokkaido radar. However, the ionospheric echoes associated with geological hazards had never been observed during previous events. Shinbori et al. (2022) studied the electromagnetic conjugate effect of ionospheric disturbances after the Tonga volcanic eruption by using observations of the GNSS-TEC and SuperDARN Hokkaido radars.

In this study, ionospheric irregularities observed by using middle-latitude SuperDARN radars and digisondes were employed as tracers to study ionospheric oscillation features in the Northern Hemisphere. Its very interesting that the ionospheric oscillation had different features before and after the arrival of the surface air pressure wave, including the maximum LOS velocity, the altitude of the maximum LOS velocity, and the propagation direction. In particular, we find that the difference of oscillation velocity in E and F layers of the ionosphere changed after the arrival of the surface air pressure wave.

2 Data

The SuperDARN is a global high frequency (HF), coherent scatter radar network that consists of more than 30 radars that observe Earth's upper atmosphere beginning at mid-latitudes and extending to polar regions in both hemispheres. There are 37 SuperDARN radars now, with 22 radars located in high-latitude and polar regions and 15 radars located in mid-latitude regions. The SuperDARN radars are sensitive to Bragg scattering from field-aligned electron density irregularities in the ionosphere (Greenwald et al., 1995). These radars operate in the HF band of the radio spectrum between 8 and 20 MHz; at these frequencies, radar signals are refracted by the ionosphere. The signals return to the radar along the same path, with the incident radar signal orthogonal to the magnetic field. The scale size of the irregularities from which the signal is scattered is equal to one-half of the radar wavelength. The HF signals are refracted toward the ground, and part of the signal may be reflected to the radar. Therefore, in addition to the backscatter received from ionosphere irregularities, SuperDARN radars receive backscatters from the ground or sea surfaces. The transmission of a multipulse scheme is used to calculate autocorrelation functions (ACFs) of the backscattered signals as a function of range. In each range gate, the ACF is analysed by a fitting routine known as FITACF that estimates the backscatter power, the LOS Doppler velocity of the irregularities and the spectral width (Ribeiro et al., 2013). A typical SuperDARN radar monitors 16 or 24 beam directions separated by 3.24 degrees in the azimuthal direction, with the 75 $\sim$ 100 range gates along each beam separated by 45 km. The dwell time of each beam is typically 2 $\sim$ 7 s (integration period), which produces a 1 $\sim$ 2 min azimuthal scan.
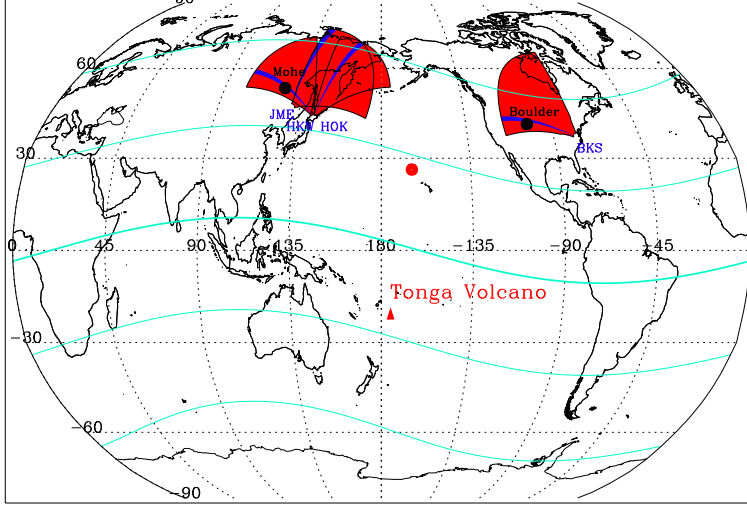
Figure 1. FOVs of the SuperDARN JME, HOK, HKW and BKS radars, with beam 0 of the JME radar and beam 4 of the HOK, HKW and BKS radars are shaded in blue. The black dots represent the locations of the Mohe and Boulder digisondes. The red triangle indicates the location of the Tonga volcano, and the red dot indicates the magnetically conjugate point of the volcano. The cyan curves indicate the magnetic latitude lines with 30 degree intervals.

The high-latitude SuperDARN radars are mainly employed to research the ionospheric convection driven by solar wind and magnetospheric interactions. Compared with radars located in high latitudes, mid-latitude radars are more suitable for research on sub-auroral phenomena and ion-neutral interactions, for example, TIDs. During the volcanic eruption in Tonga, data from four mid-latitude SuperDARN radars were available. These radars included the Jiamusi radar (JME) in China (geographic coordinates of 46.816°N, 130.402°E), the Hokkaido East radar (HOK) (geographic coordinates of 43.53°N, 143.61°E)and the Hokkaido West radar (HKW) in Japan (geographic coordinates of 43.54°N, 143.61°E), and the Blackstone radar (BKS) in the United States (geographic coordinates of 37.10°N, 77.95°W). Observations from these four radars are used to analyse the ionospheric oscillation in this study. The fields of view (FOVs) of the four radars are shown in Figure 1, where beam 0 of the JME radar and beam 4 of the HOK, HKW and BKS radars are shown in blue. The JME and BKS radars have 24 beams, while the HOK and HKW radars have 16 beams. On 15 January 2022, all four radars were operating in normal (fast) mode and sequentially sampled beams with a 2-3 s integration time for each beam; thus, the whole FOV was sampled every minute. The operating frequencies of the HOK, HKW and JME radars on 15 January 2022 were 11.07 MHz, 10.08 MHz, and 10.4 MHz, respectively. The operating frequency of the BKS radar was 10.8 MHz before 1300 UT and 11.5 MHz after 1300 UT.

The SuperDARN radars observe the LOS velocities of plasma. In addition to the SuperDARN radar data, ionogram data from two digisondes located in Mohe (geographic coordinates of 52.0° N, 122.52° E) and Boulder (geographic coordinates of 40.0°N, 105.3°W) were applied to investigate the height variations in the ionosphere. The densities and heights of the peaks of layers E, Es, F1, and F2 and electron density profiles up to 1000 km can be automatically calculated by digisondes. The Mohe ionogram data were obtained from the Chinese Meridian Project Database, and the Boulder ionogram data were obtained from the Digital Ionogram Database.

3 Results

3.1 LOS velocity observed by Four SuperDARN Radars

Range-time-intensity (RTI) plots of the LOS Doppler velocities observed by (a) beam 4 of the HOK radar, (b) beam 0 of the JME radar, (c) beam 4 of the HKW radar and (d) beam 4 of the BKS radar on 15 January 2022 are shown in Figure 2. The LOS Doppler velocities are scaled according to the colour bar shown on the right. Negative velocities represent plasma flows moving away from the radar, while positive velocities represent plasma flows moving toward the radar. The slant range is the total distance traversed by the ray between the radar and the targets. The shadow in each panel indicates night. As shown in Figure 1, beam 0 of the JME radar points to the geographical North Pole, beam 4 of the HOK radar is almost parallel to beam 0 of the JME radar, and beam 4 of the HKW and BKS radars points westward.

Before 0800 UT, backscatters with LOS velocities of less than ±30 m/s were observed by beam 4 of the HOK radar and classified as ground backscatters. Distinct ionospheric backscatters began to be observed from 0800 UT on beam 4 of the HOK radar. Plasma with negative LOS velocities were observed first, with a minimum of approximately -100 m/s, followed by a very short positive LOS velocity period with a maximum of approximately 60 m/s. Subsequently, the radar captured a second sudden transition structure with a negative LOS velocity followed by a short positive LOS velocity period, with velocity more rapid than the previous velocity. At 0900 UT, the radar observed the third negative velocity period with slower velocities than the second period, which lasted approximately one hour. From 0800 UT and 1000 UT, the location of the echoes gradually moved to a further slant range. After 1000 UT, the radar started to observe positive velocities with the location of the echoes gradually decreased to a closer slant range until 1130 UT. Beam 0 of the JME radar was approximately 1100 km west of beam 4 of the HOK radar, and the two beams were nearly parallel to each other. The radar observed similar ionospheric oscillation features with some time delay from beam 4 of the HOK radar. As shown in Figure 2(b), from 0900 UT to 1200 UT, the JME radar also observed three negative/positive velocities periods, with a relatively short duration for the first two positive velocity periods (10 minutes). The second negative/positive velocity period between 0920 UT and 1020 UT was the most rapid. The slant range of the observed echoes slowly increased from 0900 UT at approximately 500 km and rapidly dropped from a slant range of more than 1000 km at 1100 UT to a few hundreds of kilometres. Beam 4 of the HKW radar points westward. Figure 2 (c) shows the observation from beam 4 of the HKW radar is consistent with the observation from the HOK and JME radar. The positive LOS velocity regions moved to a farther slant range over time, indicating the westward propagation of the fluctuation.

Before 1130 UT, few backscatters in the slant range between 200 and 400 km (E layer of the ionosphere based on ray tracing simulations, please refer to Figure S1 in the supplemental material) were observed by beam 4 of the HOK radar. The magnitudes of the LOS velocities in this slant range were weaker than those in the slant range greater than 400 km (F layer of the ionosphere). At 1130 UT, the surface air pressure disturbances caused by the Tonga volcanic eruption arrived at the HOK radar, based on the speed of the air pressure wave of ∼340 m/s (Wright et al., 2022). Afterward, much backscatter appeared in the E region of the ionosphere, and the LOS velocities in the E region exceeded ±150 m/s and were stronger than those in the F region between 1130 UT and 1600 UT. After 1200 UT, the JME and HKW radar also observed an increase in the number of ionospheric echoes.

According to the observations of HOK and JME radar between 0800 UT and 1200 UT, the propagation direction of the ionospheric oscillation was westward. After the arrival of the surface air pressure, the propagation direction turned northwestward. Figure S2 in the supplemental material show the wavefront observed by the HOK and JME

radar at 0850 UT, 0940 UT and 1133 UT. The horizontal phase velocity was approximately 330 m/s, calculated by using the delay time and the distance between the HOK radar and the JME radar. The propagation direction and horizontal phase velocity of the ionospheric fluctuation observed by the SuperDARN radars were consistent with the observation based on TEC observations(Lin et al., 2022). SuperDARN radars in East Asia observed the strong ionospheric oscillations with three LOS velocity transitions from 0800 UT to 1200 UT, which may be attributed to the three main explosions of the volcanic eruptions in Tonga (Astafyeva et al., 2022; Wright et al., 2022). During this period, the slant range of the echoes showed a trend of rising, falling, and then rising, implying the variation in the height of the ionosphere besides the oscillation in the horizontal direction.

The BKS radar is located in the western hemisphere and under different day-night conditions during the period of interest. The backscatter received by the BKS radar was considerably different from the backscatter received by the other three radars. Almost all of the backscatter was ground scatter. The velocity variation in ground scatter for the SuperDARN radars is usually attributed to vertical movement of the ionosphere. The BKS radar received minimal backscatter before 1200 UT as the radar operating frequency and ionospheric conditions were not suitable. With sunrise, the ionosphere builds up and a band of ground scatter develops after 1230 UT. The slant range to the band varies and the LOS velocity fluctuates within narrow limits (<30 m/s) throughout the day owing to passage of TIDs, which is typical. However, after 1400 UT, ground scatter with LOS velocities greater than 90 m/s was observed by beam 4 of the BKS radar, corresponding to a marked downward motion in the ionosphere.

3.2 LOS velocity across different layers of ionosphere

To show the fluctuation velocity across different layers of the ionosphere, Figure 4 shows an RTI plot of the LOS Doppler velocity observed on beam 4 of the HOK radar and line plots of the LOS velocities of range gates 2, 4, 10, 12, 14 and 16 for beam 4 of the HOK radar, with 10 min smoothing applied. The positive/negative velocities indicate that the direction of the LOS velocity was toward/away from the radar. Range gates 2, 4, 10, 12, 14 and 16 correspond to slant ranges of 270, 360, 630, 720, 810 and 900 km, as indicated by the six black horizontal lines on Figure 3 (a). The blue vertical line at 0800 UT indicates the arrival time of the disturbance propagated from the magnetic conjugate point of the Tonga volcanic eruption, while the blue vertical line at 1130 UT indicates the arrival time of the disturbance directly propagated from the Tonga volcanic eruption. Between 0800 UT and 1130 UT, the maximum peak-to-peak amplitude of the ionospheric fluctuation velocity was approximately 150 m/s at range gate 10 (F region) and was associated with the two shock structures. During this period, the peak-to-peak amplitude observed at gate 2 (E region) was weaker than that observed in the F region. After the arrival of the surface air pressure waves at 1130 UT, the maximum LOS velocity was approximately $\pm 150 m/s$, and the peak-to-peak amplitude of the ionospheric fluctuation approached 300 m/s at range gate 4 (E region). The peak-to-peak amplitude decreased over time and as the range gate increased.

3.3 Uplift in the ionosphere by the volcanic eruption

The SuperDARN radars observed the LOS velocity of the irregularities. To investigate the vertical motion of the ionosphere, we combined the observations of beam 4 of the HKW radar and Mohe digisonde. Beam 4 of the HKW radar and the location of the Mohe digisonde are shown in Figure 1. Figure 4 shows the RTI plot of the LOS Doppler velocities observed by beam 4 of the HOK radar, the F layer peak height (hmF2) as a function of time obtained from the Mohe digisonde, and three representative ionograms to highlight the state of the ionosphere at specific times. The black horizontal dashed line in Figure 4 (a) indicates the radar slant range corresponding to the Mohe digisonde.
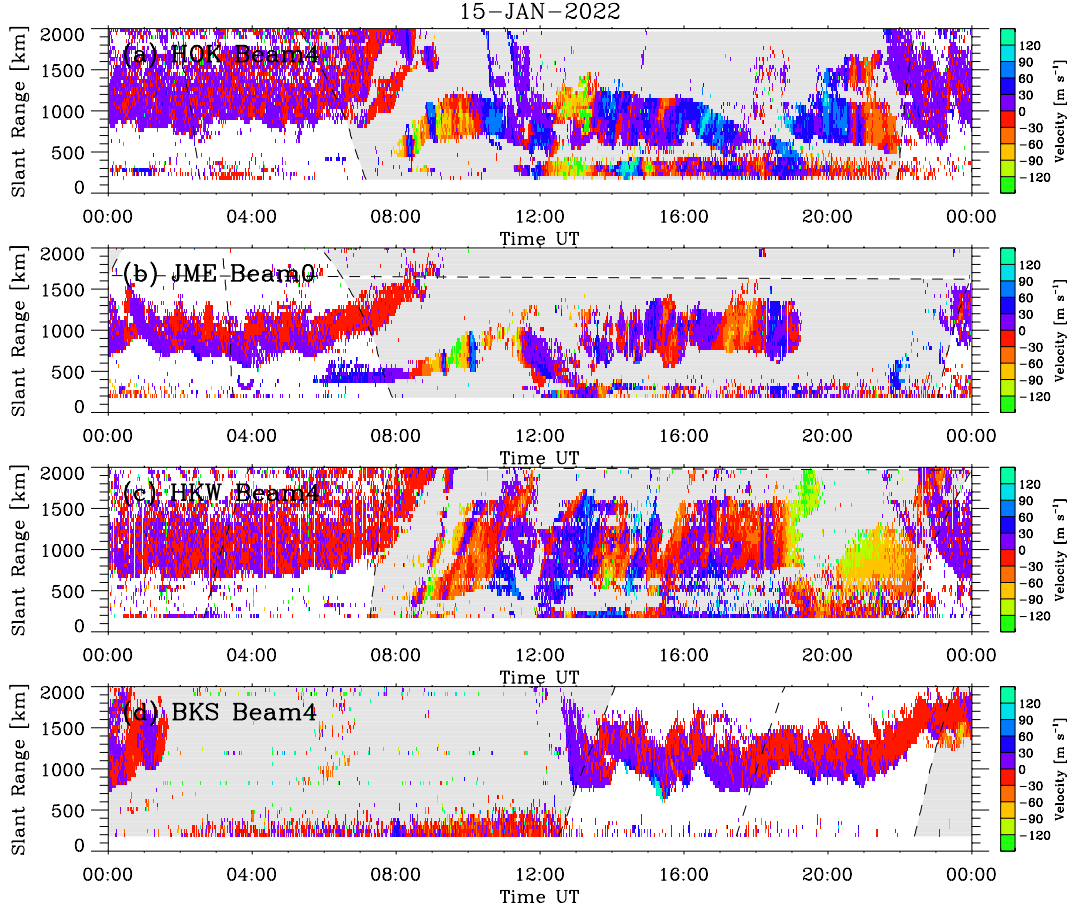
Figure 2. Range-time-intensity plots of the LOS Doppler velocities observed by (a) beam 4 of the HOK radar, (b) beam 0 of the JME radar, (c) beam 4 of the HKW radar and (d) beam 4 of the BKS radar on 15 January 2022. The LOS Doppler velocities are scaled according to the colour bar shown on the right. The shadow in each panel indicates night.
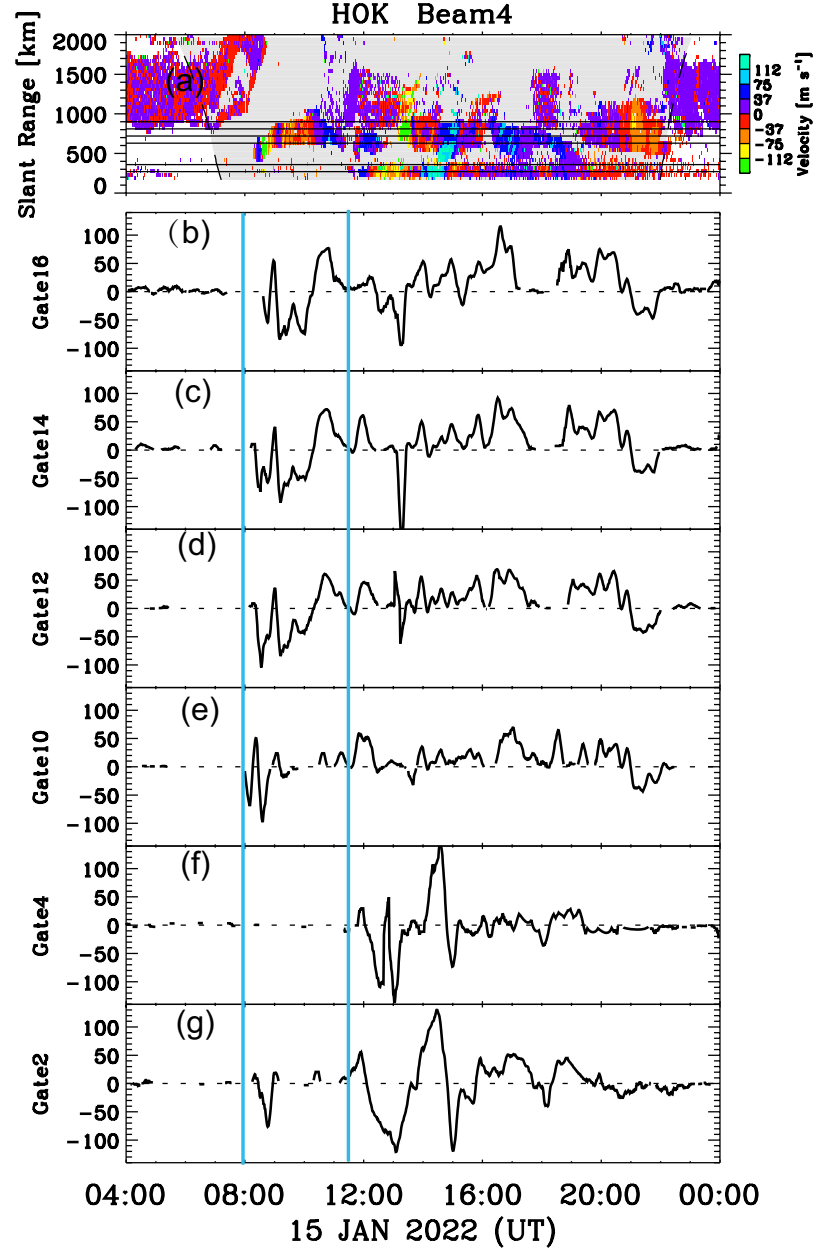
Figure 3. Fluctuation velocity across different layers of ionosphere. (a) RTI plot of the LOS Doppler velocities observed by beam 4 of the HOK radar and line plots of the LOS velocities of range gates (b)16, (c) 14, (d) 12, (e) 10, (f) 4 and (g) 2 for beam 4 of the HOK radar, with 10 min smoothing applied. Range gates 2, 4, 10, 12, 14 and 16 correspond to slant ranges of 270, 360, 630, 720, 810 and 900 km, respectively, as indicated by the six black horizontal lines in Figure 4(a). The two vertical blue lines indicate the arrival time of the disturbance from the magnetic conjugate point of the volcanic eruption in Tonga and from the volcanic eruption itself.

The two vertical blue lines in Figure 4 (a) and (b) indicate the arrival time of the disturbance to the Mohe digisonde from the magnetic conjugate point of the volcanic eruption in Tonga at 0930 UT and from the volcanic eruption itself at 1230 UT, respectively. The cyan dashed line in Figure 4 (b) indicates the variation in the peak height of the F layer during the quiet time (This is a polynomial fitting curve based on the observation during 13 Jan 2022). As shown in Figure 4, the negative/positive LOS velocities of the HKW radar correspond to the upwards/downwards motion, respectively, of the ionosphere, which were were well captured by the Mohe digisonde, indicating that the LOS velocities observed by the SuperDARN radars have a pronounced vertical component and were not purely horizontal. After the arrival of the disturbance from the magnetic conjugate point of the volcanic eruption at 0930 UT, the Mohe digisonde observed uplift of the ionosphere from 245 km to about 326 km at 1030 UT, and then the height of the ionosphere vibrated and fell to a normal height. After the disturbance from the volcanic eruption itself propagated to Mohe at approximately 1230 UT, the digisonde again observed the uplift of the ionosphere. Excluding the diurnal variation in the peak height of the F layer at the quiet time, the maximum amplitude of the vertical fluctuations caused by the volcanic eruption in Tonga was approximately 80 km, as observed by the Mohe digisonde. This finding indicates that the volcanic eruption caused strong vertical fluctuations of the ionosphere in the midlatitude region of the northern hemisphere. This vertical movement may be attributed to the fact that magnetic field lines in middle latitudes are not completely perpendicular to the ground, and so east-west electric fields in this region will produce vertical movements of the ionosphere in addition to horizontal movements.

Joint observations of beam 4 of the BKS radar and Boulder digisonde also reveal the vertical oscillation of the ionosphere (Please refer to Figure S3 in the supplemental material). The position of the Boulder digisonde is beyond the 2000 km slant range of the the BKS radar, so the location of the digisonde was not marked in the figure. A maximum positive velocity of approximately 90 m/s was observed on beam 4 of the BKS radar from 1400 UT, which correspond to a marked downward motion in the ionosphere. The Boulder digisonde also observed the rapid decrease in the peak height of the F layer from 1400 UT with an amplitude of more than 100 km, which is consistent with the observation from the BKS radar. The disturbance from the magnetic conjugate point of the volcanic eruption in Tonga and from the volcanic eruption itself arrived at the Boulder digisonde at 0905 UT and 1215 UT, respectively, which was calculated based on the speed of the air pressure wave of ∼340 m/s. Before 1400 UT, the Boulder digisonde observed the uplift and fall in the ionosphere associated with the volcanic eruption.

4 Discussion and Conclusion

According to the observation of SuperDARN radars in East Asia, the strongest LOS velocity appeared in the F layer of the ionosphere due to the magnetic field conjugate effect, and the amplitude of the velocity decreased with decreasing altitude. This finding indicates the magnetic field conjugate effect has a significant impact on the plasma flow in the F layer at another hemisphere. During this period, the ionospheric plasma flow was produced by an external electric field that is generated by an E layer dynamo in the sunlit Southern Hemisphere. The two sudden increases of the plasma flow may correspond to the two large Tonga eruption with a VEI value of 6, which can cause a significant enhancement of an E-region dynamo electric field. After the arrival of the surface air pressure wave, the strongest LOS velocity appeared in the E layer, and the amplitude of the velocity decreased with increasing altitude. During this period, the ionospheric conductivity of the E-region was very small due to the dark region, and the E layer dynamo process was not effective on the ionospheric plasma motion in the F-region. So, the E and F layer motions are directly produced by the neutral wind osculation associated with the arrival of the air pressure wave. The collision frequency is much smaller in the F layer than in the E layer. This is because the ionospheric plasma motion in
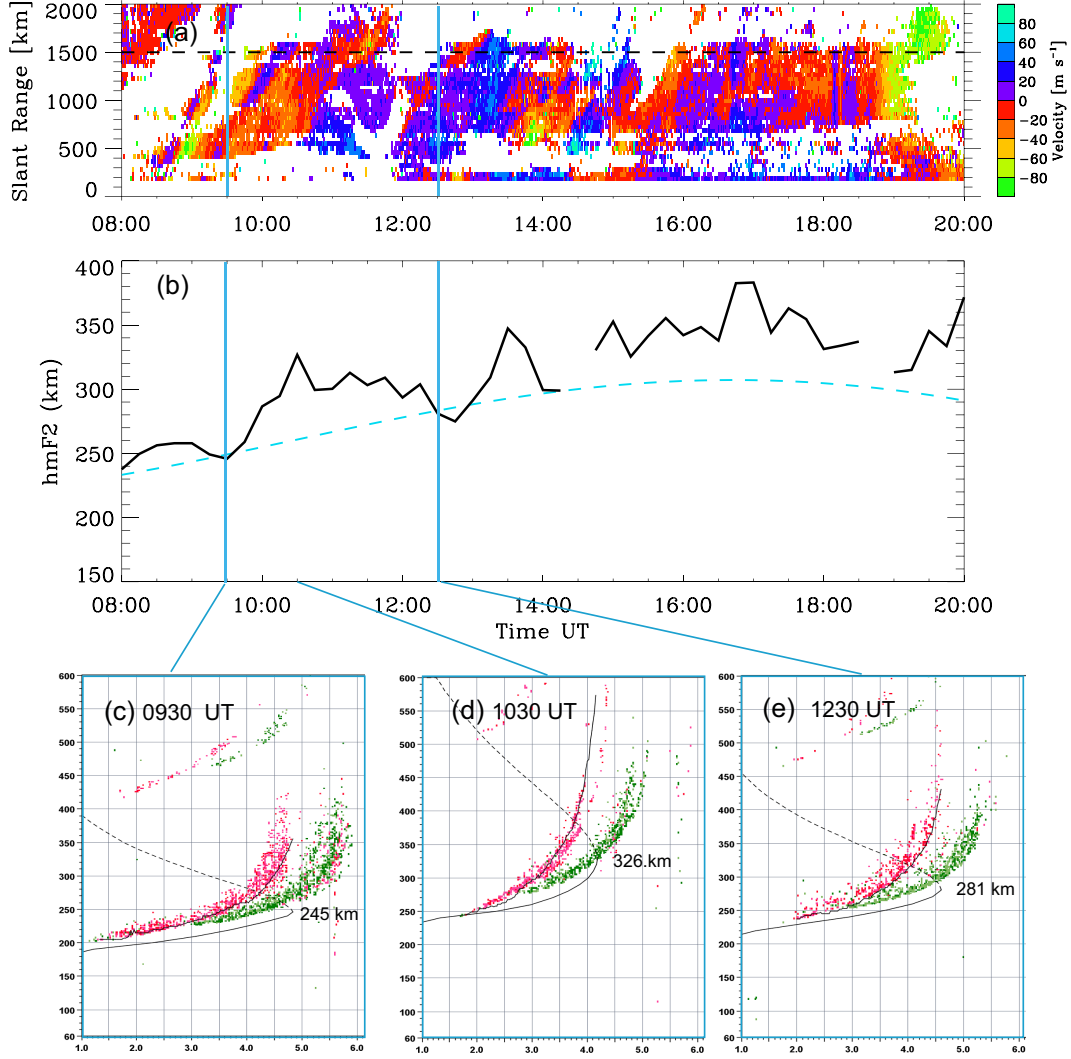
Figure 4. Vertical variation of the ionosphere. (a) RTI plot of the LOS Doppler velocities observed by beam 4 of the HOK radar. The black horizontal dashed line in panel (a) indicates the slant range corresponding to the Mohe digisonde. (b) Ionospheric peak height of the F2 layer as a function of time obtained from the Mohe digisonde. The two vertical blue lines in panel (a) and (b) indicate the arrival time of the disturbance to the Mohe digisonde from the magnetic conjugate point of the volcanic eruption in Tonga and from the volcanic eruption itself, respectively. The cyan dashed curve in panel (b) indicates the variation in the peak height of the F layer of the ionosphere during the quiet time. Three representative ionograms are shown at (c) 0930 UT, (d) 1045 UT and (e) 1230 UT.

the F layer is more decoupled with the neutral wind oscillation than in the E layer. Therefore, the plasma motion is expected to be slower in the F layer than in the E layer.

The fluctuation caused by the magnetic field conjugate effect was detected by three radars in East Asia, while the BKS radar in America did not record the fluctuation caused by the magnetic field conjugate effect. This attributed to the fact that the radar operating frequency and ionospheric conditions do not satisfy the conditions for receiving ionospheric backscatters during the relevant period. In addition, the three midlatitude SuperDARN radars in Australia and New Zealand in the Southern Hemisphere were not operating during this period. If these radars were operational, they would provide excellent observations for comparing movements in the ionosphere caused by volcanic eruptions in the Southern and Northern hemispheres, and would contribute to a deeper understanding of the mechanisms underlying the magnetic field conjugate effect.

In conclusion, impacts on ionospheric irregularities and ionospheric oscillation features in the Northern Hemisphere caused by the explosive Tonga volcanic eruption in the southwest Pacific were clearly captured by midlatitude SuperDARN radars and digisondes. The ionospheric fluctuations observed by SuperDARN radars in East Asia propagated westward due to the magnetic field conjugate effect. After the surface pressure wave arrived, the propagation direction was northwestward. The estimated propagation velocity of the ionospheric fluctuation was approximately $320 \sim 340$ m/s. The distant and upwards motion of the ionosphere was considerably more rapid and lasted longer than the forwards and downwards motion. Because of different mechanisms, the maximum peak-to-peak LOS velocity of the ionosphere exceeded 150 m/s appeared in F layer due to the magnetic field conjugate effect, and the maximum peak-to-peak LOS velocity of the ionosphere was approximately 300 m/s which appeared in the E layer due to the direct propagation of the wave from the Tonga volcano. The amplitude of the vertical rise and fall of the ionosphere in the mid-latitude region of the Northern Hemisphere can reach nearly 100 km due to the volcanic eruption. This event shows how geological hazards can impact the ionosphere and cause space weather, raising concerns for vulnerable technologies.

5 Open Research

The raw SuperDARN data are available from the SuperDARN data server at the National Space Science Center, Chinese Academy of Sciences (https://superdarn.nssdc.ac.cn/). To access the data, users should log in, and go to 'Access data' to select the radar, dataset and date. The Mohe ionogram data were obtained from the Chinese Meridian Project Database (https://data.meridianproject.ac.cn/), to access the data, users also should log in, and go to 'Download', then select 'Mohe station', and then choose 'Ionogram image of digital ionosonde'. The Boulder ionogram data were obtained from the Digital Ionogram Database (https://giro.uml.edu/didbase/).

References

Adam, D. (2022). Tonga volcano eruption created puzzling ripples in earths atmosphere [Journal Article]. *Nature*, *602*, 497. doi: https://doi.org/10.1038/d41586-022-00127-1

Astafyeva, E., Maletckii, B., Mikesell, T. D., Munaibari, E., Ravanelli, M., Cois-

son, P., . . . Rolland, L. (2022). The 15 january 2022 hunga tonga eruption history as inferred from ionospheric observations [Journal Article]. *Geophysical Research Letters*, *49*(10), e2022GL098827. Retrieved from https://agupubs.onlinelibrary.wiley.com/doi/abs/10.1029/2022GL098827 doi: https://doi.org/10.1029/2022GL098827

Carr, J. L., Horvth, k., Wu, D. L., & Friberg, M. D. (2022). Stereo plume height and motion retrievals for the record-setting hunga tonga-hunga ha'apai eruption of 15 january 2022 [Journal Article]. *Geophysical Research Letters*, *49*(9), e2022GL098131. Retrieved from https://agupubs.onlinelibrary.wiley.com/doi/abs/10.1029/2022GL098131 doi: https://doi.org/10.1029/2022GL098131

Chisham, G., Lester, M., Milan, S. E., Freeman, M., Bristow, W., Grocott, A., . . . Dyson, P. L. (2007). A decade of the super dual auroral radar network (super-darn): Scientific achievements, new techniques and future directions [Journal Article]. *Surveys in geophysics*, *28*(1), 33-109.

Dautermann, T., Calais, E., & Mattioli, G. S. (2009). Global positioning system detection and energy estimation of the ionospheric wave caused by the 13 july 2003 explosion of the soufrire hills volcano, montserrat [Journal Article]. *Journal of Geophysical Research: Solid Earth*, *114*(B2). Retrieved from https://agupubs.onlinelibrary.wiley.com/doi/abs/10.1029/2008JB005722 doi: https://doi.org/10.1029/2008JB005722

Greenwald, R. A., Baker, K. B., Dudeney, J. R., Pinnock, M., Jones, T. B., Thomas, E. C., . . . Yamagishi, H. (1995). Darn/superdarn [Journal Article]. *Space Science Reviews*, *71*(1), 761-796. Retrieved from https://doi.org/10.1007/BF00751350 doi: 10.1007/BF00751350

Heki, K. (2006). Explosion energy of the 2004 eruption of the asama volcano, central japan, inferred from ionospheric disturbances [Journal Article]. *Geophysical Research Letters*, *33*(14). Retrieved from https://agupubs.onlinelibrary.wiley.com/doi/abs/10.1029/2006GL026249 doi: https://doi.org/10.1029/2006GL026249

Lin, J.-T., Rajesh, P. K., Lin, C. C. H., Chou, M.-Y., Liu, J.-Y., Yue, J., . . . Kung, M.-M. (2022). Rapid conjugate appearance of the giant ionospheric lamb wave signatures in the northern hemisphere after hunga-tonga volcano eruptions [Journal Article]. *Geophysical Research Letters*, *49*(8), e2022GL098222. Retrieved from https://agupubs.onlinelibrary.wiley.com/doi/abs/10.1029/2022GL098222 doi: https://doi.org/10.1029/2022GL098222

Liu, C. H., Klostermeyer, J., Yeh, K. C., Jones, T. B., Robinson, T., Holt, O., . . . Kersley, L. (1982). Global dynamic responses of the atmosphere to the eruption of mount st. helens on may 18, 1980 [Journal Article]. *Journal of Geophysical Research: Space Physics*, *87*(A8), 6281-6290. Retrieved from https://agupubs.onlinelibrary.wiley.com/doi/abs/10.1029/JA087iA08p06281 doi: https://doi.org/10.1029/JA087iA08p06281

Liu, X., Xu, J., Yue, J., & Kogure, M. (2022). Strong gravity waves associated with tonga volcano eruption revealed by saber observations [Journal Article]. *Geophysical Research Letters*, *49*(10), e2022GL098339. Retrieved from https://agupubs.onlinelibrary.wiley.com/doi/abs/10.1029/2022GL098339 doi: https://doi.org/10.1029/2022GL098339

Nishitani, N., Ogawa, T., Otsuka, Y., Hosokawa, K., & Hori, T. (2011). Propagation of large amplitude ionospheric disturbances with velocity dispersion observed by the superdarn hokkaido radar after the 2011 off the pacific coast of tohoku earthquake [Journal Article]. *Earth Planets and Space*, *63*(7), 891-896.

Nishitani, N., Ruohoniemi, J. M., Lester, M., Baker, J. B. H., Koustov, A. V., Shepherd, S. G., . . . Kikuchi, T. (2019). Review of the accomplishments of mid-latitude super dual auroral radar network (superdarn) hf radars [Journal Article]. *Progress in Earth and Planetary Science*, *6*(1),

27. Retrieved from `https://doi.org/10.1186/s40645-019-0270-5` doi: 10.1186/s40645-019-0270-5

Poli, P., & Shapiro, N. M. (2022). Rapid characterization of large volcanic eruptions: Measuring the impulse of the hunga tonga haapai explosion from teleseismic waves [Journal Article]. *Geophysical Research Letters*, *49*(8), e2022GL098123. Retrieved from `https://agupubs.onlinelibrary.wiley.com/doi/abs/10.1029/2022GL098123` doi: https://doi.org/10.1029/2022GL098123

Ribeiro, A., Ruohoniemi, J., Ponomarenko, P., N Clausen, L., H Baker, J., Greenwald, R., ... Larquier, S. (2013). A comparison of superdarn acf fitting methods [Journal Article]. *Radio Science*.

Roberts, D. H., Klobuchar, J. A., Fougere, P. F., & Hendrickson, D. H. (1982). A large-amplitude traveling ionospheric disturbance produced by the may 18, 1980, explosion of mount st. helens [Journal Article]. *Journal of Geophysical Research: Space Physics*, *87*(A8), 6291-6301. Retrieved from `https://agupubs.onlinelibrary.wiley.com/doi/abs/10.1029/JA087iA08p06291` doi: https://doi.org/10.1029/JA087iA08p06291

Shinbori, A., Otsuka, Y., Sori, T., Nishioka, M., Perwitasari, S., Tsuda, T., & Nishitani, N. (2022). Electromagnetic conjugacy of ionospheric disturbances after the 2022 hunga tonga-hunga haapai volcanic eruption as seen in gnss-tec and superdarn hokkaido pair of radars observations [Journal Article]. *Earth, Planets and Space*, *74*(1), 106. Retrieved from `https://doi.org/10.1186/s40623-022-01665-8` doi: 10.1186/s40623-022-01665-8

Themens, D. R., Watson, C., ?agar, N., Vasylkevych, S., Elvidge, S., McCaffrey, A., ... Jayachandran, P. T. (2022). Global propagation of ionospheric disturbances associated with the 2022 tonga volcanic eruption [Journal Article]. *Geophysical Research Letters*, *49*(7), e2022GL098158. Retrieved from `https://agupubs.onlinelibrary.wiley.com/doi/abs/10.1029/2022GL098158` doi: https://doi.org/10.1029/2022GL098158

Wright, C. J., Hindley, N. P., Alexander, M. J., Barlow, M., Hoffmann, L., Mitchell, C. N., ... Yue, J. (2022). Surface-to-space atmospheric waves from hunga tonga-hunga haapai eruption [Journal Article]. *Nature*. Retrieved from `https://doi.org/10.1038/s41586-022-05012-5` doi: 10.1038/s41586-022-05012-5

Zhang, S.-R., Vierinen, J., Aa, E., Goncharenko, L. P., Erickson, P. J., Rideout, W., ... Spicher, A. (2022). 2022 tonga volcanic eruption induced global propagation of ionospheric disturbances via lamb waves [Journal Article]. *Frontiers in Astronomy and Space Sciences*, *9*. doi: 10.3389/fspas.2022.871275